Geol. Mag. **127** *(2), 1990, pp. 101–116. Printed in Great Britain*

The crystalline units of the High Himalayas in the Lahul–Zanskar region (northwest India): metamorphic–tectonic history and geochronology of the collided and imbricated Indian plate

U. POGNANTE*, D. CASTELLI*, P. BENNA*, G. GENOVESE*, F. OBERLI†, M. MEIER† & S. TONARINI‡

* Dipartimento di Scienze della Terra, Via Valperga Caluso 37, 10125 Torino, Italy
† Isotope Geochemistry, Swiss Federal Institute of Technology (ETH) , 8092 Zurich, Switzerland
‡ Laboratorio di Geocronologia e Geochimica Isotopica – C.N.R., Via Cardinale Maffi 36, 56100 Pisa, Italy

(*Received* 26 January 1989; *accepted* 20 June 1989)

Abstract – In the High Himalayan belt of northwest India, crustal thickening linked to Palaeogene collision between India and Eurasia has led to the formation of two main crystalline tectonic units separated by the syn-metamorphic Miyar Thrust: the High Himalayan Crystallines *sensu stricto* (HHC) at the bottom, and the Kade Unit at the top. These units are structurally interposed between the underlying Lesser Himalaya and the very low-grade sediments of the Tibetan nappes. They consist of paragneisses, orthogneisses, minor metabasics and, chiefly in the HHC, leucogranites. The HHC registers: a polyphase metamorphism with two main stages designated as M1 and M2; a metamorphic zonation with high-temperature recrystallization and migmatization at middle structural levels and medium-temperature assemblages at upper and lower levels. In contrast, the Kade Unit underwent a low-temperature metamorphism. Rb–Sr and U–Th–Pb isotope data point to derivation of the orthogneisses from early Palaeozoic granitoids, while the leucogranites formed by anatexis of the HHC rocks and were probably emplaced during Miocene time.

Most of the complicated metamorphic setting is related to polyphase tectonic stacking of the HHC with the 'cooler' Kade Unit and Lesser Himalaya during the Himalayan history. However, a few inconsistencies exist for a purely Himalayan age of some M1 assemblages of the HHC. As regards the crustal-derived leucogranites, the formation of a first generation mixed with quartzo-feldspathic leucosomes was possibly linked to melt-lubricated shear zones which favoured rapid crustal displacements; at upper levels they intruded during stage M2 and the latest movements along the syn-metamorphic Miyar Thrust, but before juxtaposition of the Tibetan nappes along the late-metamorphic Zanskar Fault.

1. Introduction

The valleys and the peaks with altitude in excess of 6000 m located between Lahul and southern Zanskar (northwest India) represent well exposed sections through a part of the High Himalayan belt which records the tectonic, metamorphic and magmatic processes linked to the continental collision of Palaeogene age between India and Eurasia. The High Himalayan crystalline rocks of northwest India have been thrust over the low-grade Lesser Himalaya Unit along the Main Central Thrust and are bounded to the northeast by the sediments of the Tibetan nappes (Fig. 1; Frank *et al.* 1973; Frank, Thoni & Purtscheller, 1977; Srikantia *et al.* 1980; Honegger *et al.* 1982; Gaetani, Garzanti & Jadoul, 1985; Searle & Fryer, 1986; Herren, 1987; Pognante *et al.* 1987; Thakur, 1987; Hodges & Silverberg, 1988; Kündig, 1989; Pognante & Lombardo, 1989; Searle & Rex, 1989; Stäubli, 1989).

In spite of the studies reported above, many areas of the High Himalayas have not been investigated in detail and some problems remain unsolved. For example, there is no general agreement as to the age of the magmatic and metamorphic processes and to the existence of major tectonic discontinuities within the High Himalayan crystalline rocks.

This paper presents new data on the geological setting, mineralogy, thermobarometry and geochronology of a little known SW–NE traverse in the Miyar and Temasa valleys from Udaipur (Chenab, Lahul) to Bardan Gompa (Zanskar) (Fig. 1) and places constraints on the possible tectonic, metamorphic and magmatic histories of the collided and imbricated Indian plate. The paper provides convincing evidence of: (1) a major syn-metamorphic discontinuity (Miyar Thrust) which developed within the High Himalayan crystalline rocks during the post-collisional Tertiary stages; (2) a metamorphic zonation linked to the Miyar Thrust; (3) a late-metamorphic discontinuity (Zanskar Fault; Herren, 1987) which truncated and/or reactivated an older thrust; (4) a polyphase

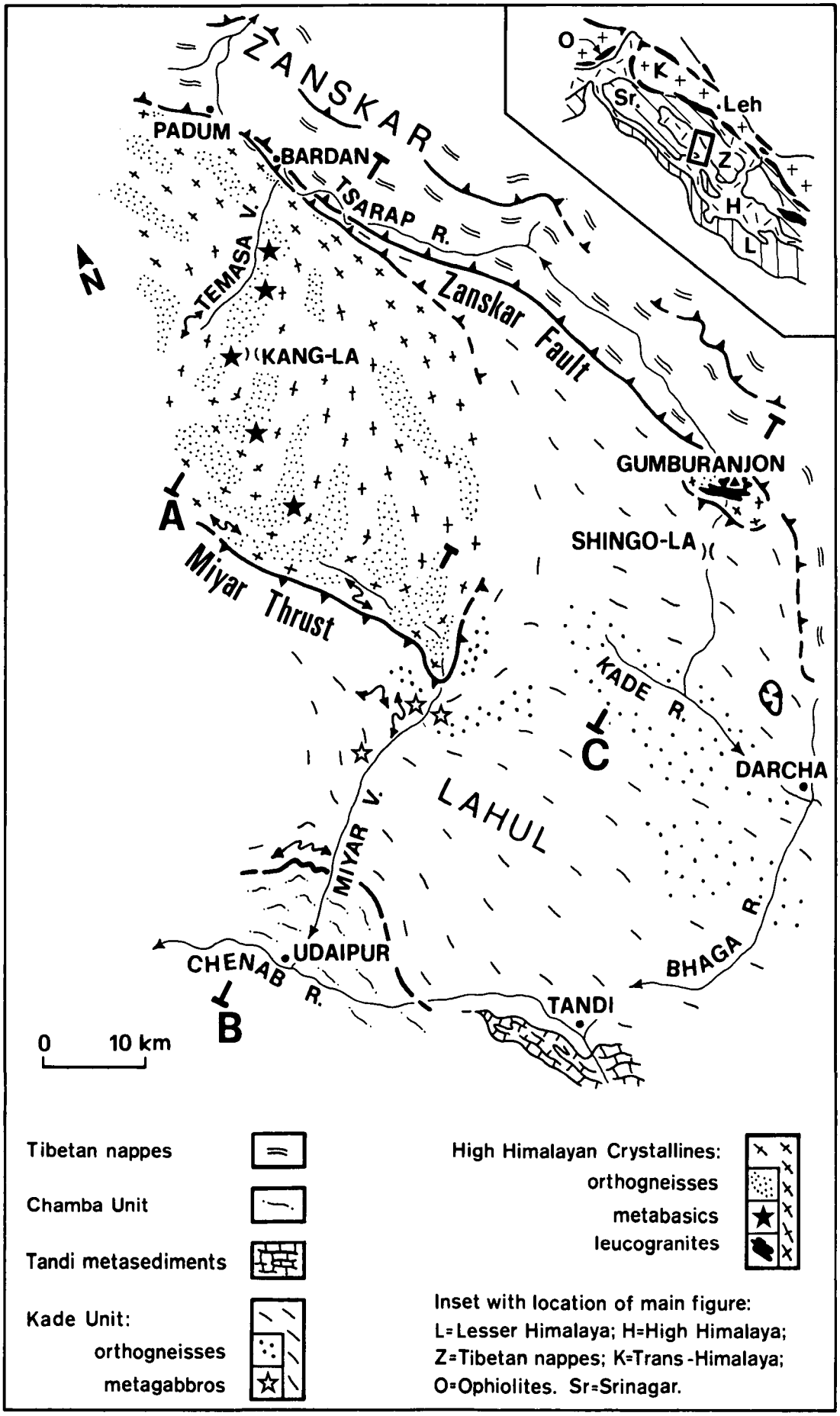

Figure 1. Geological map of the High Himalayan belt in the Lahul–Zanskar region. A, B and C indicate the cross-sections reported in Figure 2.

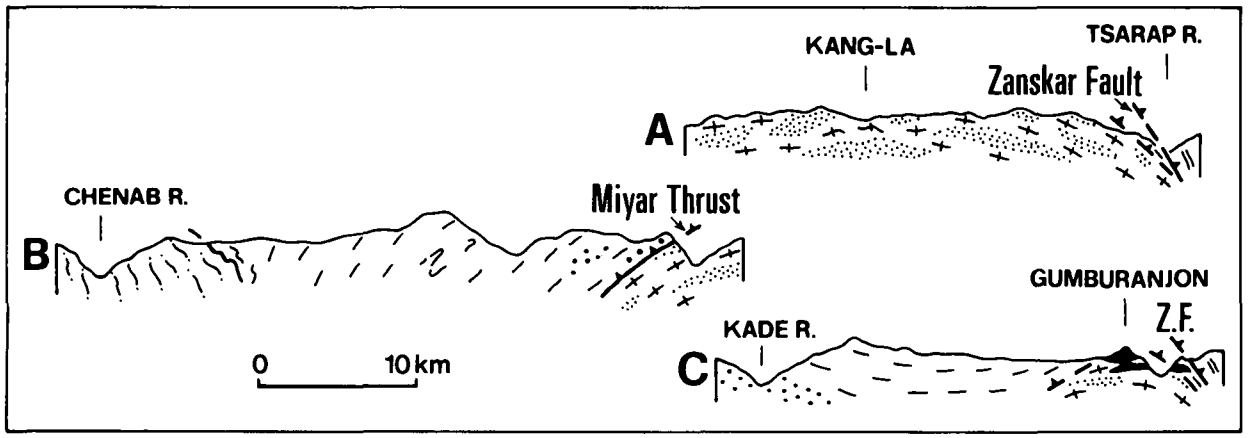

Figure 2. NE–SW cross-sections through the High Himalayan belt in the Lahul–Zanskar region. Symbols and orientations are reported in Figure 1.

intrusive history with early Palaeozoic granitoids and Tertiary leucogranites.

2. Geology and petrography

In the geological maps of the Lahul–southeast Zanskar region, the High Himalayan crystalline rocks have been usually grouped into a single, more or less coherent, structural unit (Frank *et al.* 1973; Searle, 1986; Herren, 1987; Kündig, 1989). Additionally, Thakur (1980, 1987) has recognized the 'Central Crystalline' basement and the 'Chail-Haimanta' late Precambrian to Palaeozoic cover.

Our observations partly confirm Thakur's surveys, but indicate that a major tectonic discontinuity, rather than basement–cover stratigraphic relations, exists within the High Himalayan rocks of Lahul and southeast Zanskar. Consequently two main tectonic units have been reported in the following discussion; structurally from bottom to top they have been defined as 'High Himalayan Crystallines *sensu stricto*' (HHC) and 'Kade Unit' (Figs 1 and 2). HHC and Kade Unit are separated by a syn-metamorphic thrust, hereafter designated the Miyar Thrust, while the Zanskar Fault (Herren, 1987) separates both units from the Tibetan nappes of chiefly sedimentary origin.

2.a. High Himalayan Crystallines *sensu stricto* (HHC)

Like adjacent sectors of the High Himalayan belt (Frank *et al.* 1973; Honegger *et al.* 1982; Herren, 1987; Kündig, 1989; Pognante & Lombardo, 1989; Searle & Rex, 1989; Stäubli, 1989; Treloar *et al.* 1989), the HHC consists of a sequence of paragneisses associated with orthogneisses and minor mica-schists, metabasics and leucogranites.

The *paragneisses* show a foliation defined by biotite and muscovite and consist also of quartz, plagioclase, garnet, tourmaline, Al-silicates and K-feldspar. The Al-silicates include prismatic to fibrolitic sillimanite ± kyanite in the highest-grade rocks of the middle structural levels where migmatization is widespread; sillimanite occurs in aggregates or in a fibrolitic variety which post-dates prismatic sillimanite and kyanite. In the mylonites close to the Miyar Thrust, the paragneisses are interlayered with strongly foliated mica-schists, and the metamorphic assemblages include syn-kinematic kyanite, syn-/post-kinematic staurolite with rare post-kinematic fibrolite.

The *orthogneisses* form up to kilometre-sized bodies and transposed intercalations derived from stocks and dykes of granitoids. They consist of quartz, plagioclase, K-feldspar, micas, tourmaline and garnet. Abundant centimetre-sized aggregates of sillimanite ± biotite occur in some migmatized and banded orthogneisses characterized by biotite-rich foliated melanosomes and concordant or discordant quartzofeldspathic leucosomes rich in tourmaline; in places the leucosomes gradually transform to and are mixed with leucogranites. The sillimanite-biotite aggregates and K-feldspar are partly replaced by muscovite and quartz.

Two types of *metabasic* rocks have been recently recognized in the HHC of southeast Zanskar by Pognante & Lombardo (1989). A first type of metabasic rock is intruded by the granitoids, later transformed to orthogneisses, and shows rare relics of an early clinopyroxene–garnet–plagioclase–quartz-bearing assemblage replaced by a typical amphibolite–facies assemblage. The granitoids in turn are intruded by a second type of metabasic rock which locally shows relics of magmatic minerals (clinopyroxene, plagioclase, orthopyroxene and pseudomorphed olivine) and is characterized by a metamorphic mineralogy consisting of amphiboles, plagioclase, biotite, sphene, minor garnet and, notably in the high-grade zone of the upper Miyar Valley, neoblastic orthopyroxene.

Leucogranites and *pegmatites* form both concordant layers which mix with the leucosomes of the migma-

tized gneisses, and dykes or lens-shaped bodies which crosscut the main regional foliation; dykes and bodies intrude both the leucosomes of the migmatized gneisses and, perhaps, a first generation of concordant leucogranites which may have sustained ductile deformation under partly molten conditions. The leucogranites are less abundant than the orthogneisses, while the main intrusive body occurs at the top of the HHC near Mt Gumburanjon (Fig. 1; Pognante *et al.* 1987). The leucogranites usually lack a pervasive metamorphic foliation, have a marked grain-sized variation from very coarse- to fine-grained varieties and consist of quartz, plagioclase, K-feldspar, biotite, muscovite, tourmaline and garnet.

2.b. Kade Unit

Though distribution of the Kade Unit partly corresponds to the 'Chail-Haimanta' cover of Thakur (1980, 1987), it has been defined as a more or less coherent tectonic element for the first time in this paper. It outcrops in the Miyar Valley and in the Kade Chu–Shingo La area, while it thins out northwestward. The Kade Unit consists of low-grade *metagreywackes* and *metapelites* including albite, biotite, garnet ± epidote, which are intruded by up to kilometre-sized plutons and dykes of K-feldspar-bearing granitoids transformed into *orthogneisses*. *Metagabbros* characterized by relics of brown hornblende and ophitic or porphyritic structures, and rare *metacumulates* preserving cumulus olivine and spinel with intercumulus plagioclase and clinopyroxene, are associated with the orthogneisses; the metamorphic recrystallization produced green amphibole, biotite and epidote together with re-equilibration of plagioclase toward albitic compositions. Rare deformed pegmatites and leucogranites occur close to the Miyar Thrust. Leucogranite intrusions in the Kade Unit are probably more abundant near Mt Gumburanjon (Figs 1 and 2). Unfortunately in this area the metapelites are coarse-grained and similar to the HHC paragneisses and hence the exact location of the HHC–Kade Unit boundary is not evident; such a marked recrystallization of the Kade Unit rocks, with scattered formation of biotite ± garnet centimetric porphyroblasts and amphibole–plagioclase veins, is tentatively ascribed to emplacement of the Gumburanjon leucogranite body.

2.c. Miyar Thrust

The Miyar Thrust is a shear zone very well exposed in the Miyar Valley, where it dips 30–45° southwestward (Figs 1 and 2). Here it is up to a few tens of metres thick and separates the Kade Unit from the HHC. Kyanite–staurolite- and garnet–biotite-bearing mylonites occur along this boundary in the HHC and in the Kade Unit, respectively. Transposed orthogneiss layers and intrafolial folds, but also folded or concordant leucogranites, have been observed within the shear zone. In the Gumburanjon area the Miyar Thrust has different characteristics and the mylonitic structure and minerals have been partly obliterated. As discussed in section 2.b, this may be ascribed to intrusion of the Gumburanjon leucogranite pluton at a high structural level of the HHC and probably even in the Kade Unit. In conclusion the Miyar Thrust should be considered a relatively deep-seated syn-metamorphic shear zone which was roughly coeval with, or just pre-dated, intrusion of the last generation of leucogranites; it is related to the thrust of the 'cold' Kade Unit over the 'hot' HHC.

2.d. Zanskar Fault

The Zanskar Fault is a late-metamorphic discontinuity occurring along the Tsarap and Kurgiakh-Chu rivers in southeast Zanskar (Fig. 1). It dips 45–55° northeastward and defines the boundary between the HHC (or thinned sections of the Kade Unit) and the Tibetan nappes (Fig. 2). According to Herren (1987) and Searle & Rex (1989), the Zanskar Fault is directly linked to extensional tectonics at upper crustal levels and to structural telescoping of the metamorphic isograds. Additionally, our observations indicate that an incipient syn-tectonic recrystallization, producing fine-grained muscovite ± chlorite ± biotite, is localized in the fault zone; in the HHC rocks, these minerals form films that anastomose around porphyroclasts of the pre-existing assemblages, notably garnet, staurolite, kyanite, K-feldspar and large biotite or muscovite flakes. Finally, leucogranites are deformed in the fault zone and are lacking in the Tibetan nappes. These lines of evidence suggest that the Zanskar Fault post-dates leucogranite intrusion and actually records a shallow-level tectonism which reactivated or truncated at low angle an older syn-metamorphic shear zone comparable to the Miyar Thrust. This is consistent with the apparent thinning of the Kade Unit from the Tandi–Shingo La area to the Bardan–Padum area (Fig. 1).

3. Mineral chemistry

Mineral compositions of the studied rocks have been obtained with an ARL-SEMQ microprobe, while representative compositions of the main minerals are reported in Tables 1 and 2. Location and mineralogy of the analysed samples are reported in Appendix B. Chemical analyses have been recalculated using a computer program (Ulmer, 1986) which assigns cations by different procedures as denoted in each table.

3.a. Pyroxenes

Table 1 and Figure 3 report analyses of clino- and orthopyroxenes from metabasic rocks occurring in the

Table 1. Representative microprobe analyses of pyroxenes and garnets

Unit & Sample	Clinopyroxenes		Orthopyroxenes			Garnets					
	Middle HHC (V1637)					Kade Unit (V1678)		Top HHC (V1726)		Middle HHC (V1731)	
	core	rim	core	rim	metam.	core	rim	core	rim	core	rim
SiO_2	50.53	52.10	54.88	54.22	53.89	37.13	37.29	37.18	37.10	36.77	36.62
TiO_2	1.17	0.35	0.31	0.02	0.00	0.02	0.00	0.05	0.06	0.00	0.00
Cr_2O_3	0.64	0.52	0.12	0.12	0.18	0.04	0.00	0.01	0.02	0.00	0.05
Al_2O_3	5.10	3.35	1.83	2.56	2.28	20.34	20.67	20.50	20.61	20.03	20.36
Fe_2O_3	3.64	1.53	0.75	0.91	1.58	0.95	0.69	0.80	0.65	1.17	0.47
FeO	1.77	2.83	11.01	13.18	13.11	32.90	33.60	31.48	34.09	30.54	30.89
MnO	0.17	0.13	0.25	0.37	0.29	3.96	4.03	4.62	2.10	8.96	9.29
MgO	15.65	15.48	29.72	27.89	28.34	2.98	3.14	2.17	2.86	1.77	1.37
CaO	19.88	22.67	1.22	0.91	0.22	1.64	1.04	3.47	2.44	0.87	0.75
Na_2O	1.33	0.65	0.02	0.09	0.05	n.d.	n.d.	n.d.	n.d.	n.d.	n.d.
Total	99.88	99.61	100.12	100.27	99.95	99.95	100.46	100.28	99.92	100.12	99.81
Si	1.846	1.912	1.943	1.935	1.930	3.003	2.999	2.999	2.995	3.003	3.003
Al^{iv}	0.154	0.088	0.057	0.065	0.070	0.000	0.001	0.001	0.005	0.000	0.000
Al^{vi}	0.065	0.057	0.019	0.042	0.026	1.939	1.958	1.948	1.956	1.928	1.968
Ti	0.032	0.010	0.008	0.000	0.000	0.001	0.000	0.003	0.004	0.000	0.000
Cr	0.018	0.015	0.003	0.003	0.005	0.003	0.000	0.001	0.001	0.000	0.003
Fe^{3+}	0.100	0.042	0.020	0.024	0.043	0.058	0.042	0.048	0.039	0.072	0.029
Fe^{2+}	0.054	0.087	0.326	0.393	0.393	2.225	2.259	2.124	2.301	2.086	2.119
Mn	0.005	0.004	0.008	0.011	0.009	0.271	0.274	0.316	0.144	0.620	0.645
Mg	0.852	0.847	1.568	1.484	1.513	0.359	0.376	0.261	0.344	0.216	0.168
Ca	0.778	0.892	0.046	0.035	0.009	0.142	0.090	0.300	0.211	0.076	0.066
Na	0.094	0.046	0.001	0.006	0.004	—	—	—	—	—	—

Structural formulae have been calculated on the basis of: 4 cations and 6 oxygens for pyroxenes; 8 cations and 12 oxygens for garnets. Fe^{3+} contents have been computed assuming stoichiometry and charge balance; n.d. = not detected. Pyroxene analyses refer to partly re-equilibrated magmatic compositions except for analysis 'metam' which has been carried out on a neoblastic grain.

high-grade zone of the HHC which derives from a pre-Himalayan gabbro-norite. Clinopyroxenes are zoned diopsides with cores of presumably magmatic origin enriched in Al, Ti and Cr relative to the re-equilibrated rims. Orthopyroxenes are bronzites and form coarse-grained magmatic relics enriched in Mg, Ti, Ca with respect to partly re-equilibrated rims and to small neoblastic grains. Clinopyroxenes from other types of HHC metabasic rocks have been studied in detail by Pognante & Lombardo (1989).

3.b. Garnets

Analyses of garnets from gneissic rocks are reported in Table 1 and Figure 3, and are characterized by Fe-rich compositions. In the Kade Unit and at the top of the HHC, garnets are zoned and display cores enriched in Ca and depleted in Mg and Fe relative to the rims. In contrast, garnets from the middle levels of the HHC are more homogeneous and have cores slightly enriched in Mg relative to the rims.

3.c. Micas

Table 2 shows that the analysed micas are muscovites and biotites. Biotites are enriched in Fe relative to Mg (except for metabasic rock V1637) and are characterized by high Ti contents.

3.d. Plagioclases

Plagioclases are albites (an = 6–8 mol%) in the Kade Unit and oligoclases (an = 15–23 mol%) in the HHC gneisses. In the Kade Unit and at the top of the HHC, plagioclases show a more or less distinct inverse zoning, while in the middle levels of the HHC they have more homogeneous compositions. Plagioclases analysed in metabasic rock V1637 have a marked compositional heterogeneity ranging from labradorites (an = 53 mol%) in reaction coronas rimming orthopyroxene, to bytownites (an = 87 mol%).

3.e. Other minerals

Table 2 reports analyses of two amphiboles and one zoned staurolite of the HHC. Amphiboles have been analysed in metabasic sample V1637 and, according to the IMA classification (Leake, 1978), are pargasitic- or edenitic-hornblendes. Staurolite occurs in a mylonitic gneiss close to the Miyar Thrust and is a Fe-rich variety characterized by cores slightly depleted in Fe relative to the rims.

4. Metamorphic evolution and thermobarometry

The main metamorphic assemblages and the *P–T* values estimated from thermobarometry are reported

Table 2. Representative microprobe analyses of micas, amphiboles and staurolites

Unit & sample	Muscovites				Biotites				Amphiboles		Staurolites	
							Middle HHC				Top HHC (V1726)	
	Kade Unit (V1678)	Top HHC (V1726)		Middle HHC (V1637)	Kade Unit (V1678) rim	Top HHC (V1726) rim	(V1731) core	(V1637) core	(V1637)		core	rim
SiO_2	47.02	47.40	46.92	48.48	36.49	35.55	34.34	38.18	44.98	46.49	28.66	28.57
TiO_2	0.48	0.34	0.55	0.00	2.08	1.86	2.38	4.66	0.08	0.64	0.63	0.42
Cr_2O_3	0.03	0.00	0.04	0.02	0.03	0.00	0.04	0.24	0.01	0.36	0.00	0.00
Al_2O_3	35.35	35.75	35.78	34.51	19.35	20.30	18.94	14.69	13.48	10.67	54.16	54.25
Fe_2O_3	n.c.	n.c.	n.c.	n.c.	n.c.	n.c.	n.c.	n.c.	5.84	4.44	n.c.	n.c.
FeO	1.17	0.99	1.09	0.73	19.31	19.76	25.22	9.03	1.39	3.98	12.64	13.07
MnO	0.06	0.01	0.00	0.01	0.19	0.10	0.39	0.00	0.14	0.05	0.33	0.36
MgO	0.77	0.65	0.50	1.43	9.62	9.08	5.53	18.77	17.13	16.52	1.33	1.29
CaO	0.00	0.00	0.00	0.00	0.00	0.00	0.00	0.00	11.99	11.94	0.00	0.00
Na_2O	1.15	1.02	0.96	0.08	0.47	0.33	0.20	0.80	2.32	1.62	n.d.	n.d.
K_2O	8.96	9.00	9.39	10.02	8.40	9.11	9.33	9.40	0.95	1.09	n.d.	n.d.
H_2O	4.56	4.57	4.55	4.59	3.92	3.90	3.77	4.05	2.12	2.10	2.17	2.17
Total	99.55	99.73	99.78	99.87	99.86	99.99	100.14	99.82	100.44	99.90	99.92	100.15
Si	3.092	3.105	3.087	3.165	2.791	2.734	2.727	2.822	6.345	6.629	7.902	7.877
Al^{iv}	0.908	0.895	0.913	0.835	1.209	1.266	1.273	1.178	1.655	1.371	n.c.	n.c.
Al^{vi}	1.832	1.865	1.862	1.819	0.535	0.574	0.500	0.101	0.587	0.422	17.598	17.626
Ti	0.000	0.017	0.027	0.000	0.120	0.108	0.142	0.259	0.008	0.069	0.131	0.087
Cr	0.002	0.000	0.002	0.001	0.002	0.000	0.002	0.014	0.001	0.041	0.000	0.000
Fe^{3+}	n.c.	n.c.	n.c.	n.c.	n.c.	n.c.	n.c.	n.c.	0.620	0.476	n.c.	n.c.
Fe^{2+}	0.064	0.054	0.060	0.040	1.235	1.271	1.675	0.558	0.164	0.474	2.914	3.013
Mn	0.003	0.001	0.000	0.001	0.012	0.006	0.026	0.000	0.017	0.006	0.077	0.084
Mg	0.076	0.064	0.049	0.139	1.097	1.041	0.655	2.068	3.603	3.512	0.547	0.530
Ca	0.000	0.000	0.000	0.000	0.000	0.000	0.000	0.000	1.812	1.824	0.000	0.006
Na	0.147	0.130	0.122	0.010	0.070	0.049	0.031	0.115	0.635	0.448	—	—
K	0.752	0.752	0.788	0.834	0.819	0.894	0.945	0.886	0.171	0.198	—	—
OH	2.000	2.000	2.000	2.000	2.000	2.000	2.000	2.000	2.000	2.000	4.000	4.000

Structural formulae have been calculated on the basis of: 6 cations and 12 oxygens for muscovites; 7 cations and 12 oxygens for biotites, 13 cations (N_{cat}–Ca–Na–K = 13) and 24 oxygens for amphiboles; 48 oxygens for staurolites. The H_2O wt % have been calculated from OH content derived from stoichiometry; Fe^{3+} in amphiboles has been computed assuming stoichiometry and charge balance; n.c. = not calculated; n.d. = not detected.

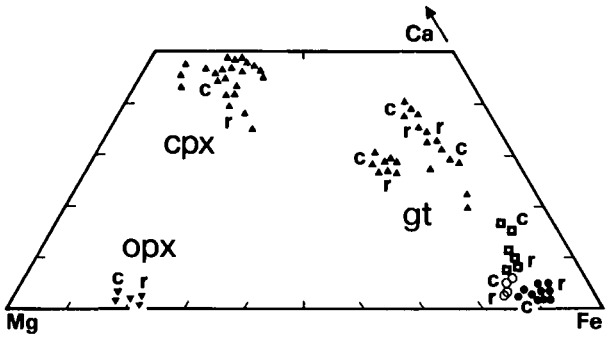

Figure 3. Ca–Mg–Fe diagram of garnets and pyroxenes (mol %). Clinopyroxenes (▲) and orthopyroxenes (▼) from HHC metabasics; garnets from HHC metabasics (▲); garnets from the sillimanite-bearing high-grade gneisses of the HHC (●), the kyanite-staurolite-bearing gneisses from the top of the HHC (□) and the biotite-bearing gneisses of the Kade Unit (○). c: core and r: rim compositions.

in Table 3 for rocks of the Kade Unit and of the upper and middle structural levels of the HHC.

In the HHC two main metamorphic stages, defined as M1 and M2, have been recognized on the basis of microstructural relationships, but they are not necessarily exactly coeval at different structural levels. Particularly, M1 might include both pre-Himalayan and Himalayan assemblages (see below). A further incipient metamorphic recrystallization M3 produced fine-grained muscovite ± biotite ± chlorite and is localized in the mylonites and cataclasites of the Zanskar Fault zone.

Geothermometric estimates have been obtained employing the Fe-Mg exchange equilibria in garnet-biotite pairs with the Ferry & Spear (1978) calibration, and the Fe–Mg exchange equilibria in garnet–clinopyroxene pairs with the Ellis & Green (1979) calibration, while pressures have been derived using the gt–pl–AS–qtz barometer of Newton & Haselton (1981) and the gt–pl–cpx–qtz barometer of Newton & Perkins (1982). The estimates are reported in Table 3 for core and rim mineral compositions in order to provide constraints for the *P–T* evolution. However, for reconstruction of *P–T* histories, interpretation of zoning considering the growth and diffusional models reviewed by Tracy (1982) is required. The higher Mg/Fe ratio of garnet cores relative to rims in the high-grade gneisses is consistent with post-growth volume diffusion during a *P–T* decrease. In contrast, the Ca enrichment and the lower Mg/Fe ratio in garnet cores relative to rims, and the inverse zoning pattern of plagioclase in the low-grade gneisses of the Kade Unit and at the top of HHC, are suggestive of growth zoning during a prograde evolution.

Thermobarometric estimates of the HHC confirm with rather good approximation the metamorphic evolution inferred by phase equilibria (Fig. 4) and microstructure. In the middle structural levels of the

Table 3. Metamorphic assemblages and thermobarometry of the crystalline rocks from the Lahul–Zanskar region

Rock types	Metamorphic assemblages		Thermobarometry based on core and rim compositions of M1 assemblages	
			Core	Rim
Kade Unit				
pgn	ms–bi–ab ± gt ± ep		$T = 560 \pm 10$ °C(1)	$T = 580 \pm 15$ °C(1)
ogn	ms–bi–ab ± gt			
mb	bi–ab–am ± ep			
Top of the HHC				
	M1	M2		
pgn	ms–bi–pl–gt–ky–st	bi–ms ± sill ± st	$T = 520 \pm 30$ °C(1) $P = 7.5 \pm 1.0$ kbar(2)	$T = 580 \pm 20$ °C(1) $P = 6.5 \pm 0.5$ kbar(2)
ogn	bi–ms–pl–kf–gt	bi–pl		
mb	cpx–hbl–gt–pl ± qtz	hbl–pl–bi		
Middle structural levels of the HHC				
	M1	M2		
pgn	bi–pl–sill–gt ± ky ± kf	ms–bi–pl–sill	$T = 700 \pm 60$ °C(1) $P = 6.6 \pm 0.7$ kbar(2)	$T = 610 \pm 70$ °C(1) $P = 5.2 \pm 1.0$ kbar(2)
ogn	bi–pl–sill–kf ± gt	ms–bi–pl		
mb	hbl–pl–gt ± bi/ cpx–gt–qtz–pl–hbl/ hbl–pl–opx–bi	bi–hbl–pl	$T = 770 \pm 40$ °C(3)* $P = 12.0 \pm 0.5$ kbar(4)*	$T = 750 \pm 50$ °C(3)* $P = 9.5 \pm 0.5$ kbar(4)*

Abbreviations: pgn = paragneisses and micaschists; ogn = orthogneisses; mb = metabasics. Thermobarometers: (1) = gt–bi, Ferry & Spear (1978); (2) = gt–pl–AS–qtz, Newton & Haselton (1981); (3) = cpx–gt, Ellis & Green (1979); (4) = gt–pl–cpx–qtz, Newton & Perkins (1982). *Reported by Pognante & Lombardo (1989).

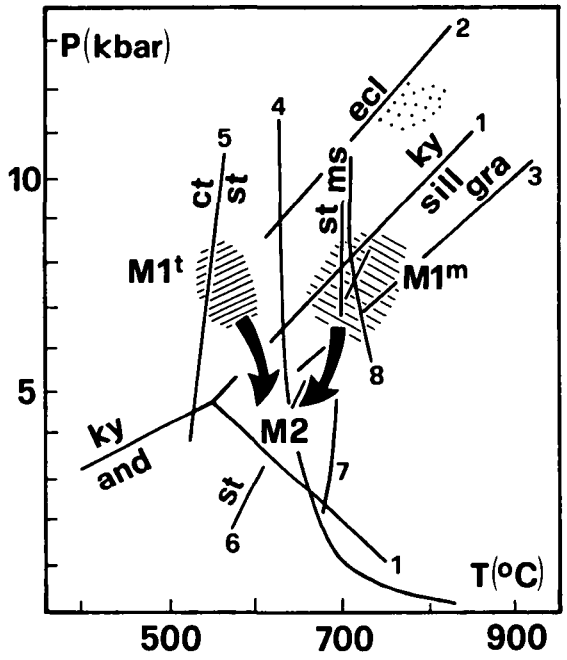

Figure 4. *P–T* grid to show the suggested conditions of metamorphism and *P–T* paths of the High Himalayan Crystallines *sensu stricto* (HHC) in the Lahul–Zanskar region. $M1^t$ and $M1^m$ are the early stages of metamorphism in the upper and middle structural levels of the HHC, respectively. Dotted area indicates the possible conditions of the early (pre-Himalayan?) metamorphism in some HHC metabasics. Curves: 1 = and–ky–sill stability fields (reported by Mueller & Saxena, 1977); 2, 3 = low-*P* stability fields of eclogite and gt-granulite in qtz-tholeiitic compositions (Green & Ringwood, 1967); 4 = ab–Kf–qtz–H_2O system, beginning of melting (Merrill, Robertson & Wyllie, 1970); 5 = ct + ky ⇌ st + alm + H_2O (Rao & Johannes, 1979); 6 = st + ms + qtz ⇌ AS + bi + H_2O (Hoschek, 1969); 7 = Fe–st + qtz ⇌ Fe–gt + sill + H_2O (Richardson, 1968); 8 = Kf + qtz + ms + H_2O ⇌ L (Storre & Karotke, 1971).

HHC the early stage M1 occurred at $T = 650$–750 °C and $P = 6$–8 kbar and was followed by an incomplete recrystallization M2 at decreasing temperature and pressure. In contrast, at the top of the HHC near the Miyar Thrust, the mylonites record an early recrystallization M1 at $T = 500$–600 °C and $P = 6$–8 kbar followed by a drop in pressure at more or less increasing temperature (M2). Interpretation of *P–T* estimates in some polyphase metabasics described by Pognante & Lombardo (1989) is more complex. For these metabasics the higher pressure values (≈ 12 kbar at $T \approx 750$ °C) suggested by the gt–pl–cpx–qtz barometer relative to pressures obtained in the gneisses, reflect either disequilibrium between the involved phases or an older (pre-Himalayan?) metamorphic stage not preserved in the gneisses. The orthopyroxene-bearing metamorphic assemblage observed in some metabasics from the high-grade zone of the HHC (Table 3) is suggestive of medium/low-pressure granulite conditions.

The metamorphic evolution proposed here for the HHC is only partly similar to those inferred by Kündig (1989) and Stäubli (1989) in more westerly sectors of Zanskar; these authors ascribed the highest temperature assemblages of the middle structural levels to M2 rather than to M1, while their temperature estimates are 50–100 °C lower than our values and probably reflect a more evident readjustment of garnet-biotite exchange equilibria during retrogression.

As regards the Kade Unit, the estimates which point to $T \approx 550$–600 °C are probably too high and are not wholly consistent with the greenschist-facies assemblages including clinozoisite and albitic plagioclase; however, these *P–T* values have been obtained in rocks from the Miyar Thrust (where clinozoisite is lacking) and may testify to 'heating' of the Kade Unit approaching the 'hot' HHC. A similar metamorphic zonation has been observed by Stäubli (1989) at the base of the HHC near the tectonic boundary with the Lesser Himalaya of the Kishtwar window.

5. Geochronology

Rb–Sr and U–Th–Pb isotope analyses have been carried out in order to derive constraints on the age of the Kade Unit and HHC granitoids. This has yielded rather coherent data for metagranitoids of the Kade Unit and slightly migmatized orthogneisses of the HHC, while heterogeneous Sr isotopic ratios in whole-rock analyses and inherited radiogenic lead in zircons make age dating difficult in the leucogranites and in the migmatized orthogneisses. For the leucogranites, a Tertiary, probably Miocene, age is defined by mica cooling ages (see section 5.a) and geological constraints (see section 2.a).

5.a. Rb–Sr isotope data

Chemical compositions and Rb–Sr analytical data for rocks of the Kade Unit are given in Tables 4 and 5. The analysed samples are: five K-feldspar-bearing

Table 4. Chemical compositions of the rocks of the Kade Unit selected for Rb–Sr dating

Sample	K1	K2	K3	K4	K6	K7
SiO_2	67.22	69.11	68.88	48.82	72.23	70.07
TiO_2	0.49	0.45	0.45	0.57	0.20	0.41
Al_2O_3	15.22	14.57	14.72	17.55	15.17	15.52
Fe_2O_3	0.85	0.71	0.81	1.15	0.65	0.73
FeO	2.96	2.63	2.55	7.12	0.89	2.17
MnO	0.07	0.07	0.06	0.16	0.03	0.06
MgO	2.55	2.10	2.10	8.86	0.47	1.02
CaO	2.95	2.37	2.38	12.24	0.39	0.88
Na_2O	2.54	2.68	2.74	1.83	2.99	2.49
K_2O	4.27	4.41	4.38	0.32	5.52	5.25
P_2O_5	0.14	0.14	0.14	0.06	0.23	0.22
L.O.I.	0.74	0.76	0.79	1.32	1.25	1.22

L.O.I. = loss on ignition. Totals have been normalized to 100.

Table 5. Rb–Sr analytical data and whole-rock biotite age for the rocks of the Kade Unit reported in Table 4

Sample	Rb (ppm)	Sr (ppm)	$^{87}Rb/^{86}Sr$	$^{87}Sr/^{86}Sr \pm 2\sigma$	Age (Ma)
K1 WR	259	131	5.74	0.76015±19	
K1 Bi	1083	1.22	2772	1.54783±95	20.0±0.3
K2 WR	239	116	6.01	0.76434±15	
K3 WR	231	128	5.22	0.76027±6	
K4 WR	13	97.5	0.39	0.71322±9	
K6 WR	415	51.8	23.63	0.90201±21	
K7 WR	324	71.6	13.25	0.82129±22	

Analytical uncertainty of $^{87}Rb/^{86}Sr$ ratios are ±1.5%. The decay constant used for ^{87}Rb is 1.42×10^{-11} g^{-1} as recommended by Steiger & Jäger (1977). $^{87}Sr/^{86}Sr$ ratios have been normalized to $^{88}Sr/^{86}Sr = 0.1194$. The Sr results were adjusted to a value of .71026 for NBS SRM 987.

orthogneisses (K1, K2, K3, K6 and K7) and one amphibole-bearing metagabbro (K4). The whole-rock data of the five orthogneiss samples define a rectilinear array (MSWD = 36.7) corresponding to an age of 549±70 Ma and an initial $^{87}Sr/^{86}Sr$ ratio of 0.7175± 0.0073 (uncertainties of age and intercept at 95% confidence level and are multiplied by Student's *t*; Ludwig, 1988). In view of the rather high MSWD value, the age result approximates rather than defines the age of granite emplacement. The data, however, preclude a Himalayan origin for the orthogneisses and furnish evidence for a period of early Palaeozoic magmatism. Combining the same five orthogneiss sample data with those of metagabbro K4, Ferrara *et al.* (1987) have obtained a preliminary isochron of 614±36 Ma. The very high MSWD value of 107 resulting from the best-fit of the combined data, however, suggests that metagabbro K4 might well have undergone a separate evolution and therefore should not be pooled with the orthogneisses (Fig. 5).

The Rb–Sr whole-rock age and the initial $^{87}Sr/^{86}Sr$ ratio are in the range of Rb–Sr ages measured in adjacent metagranitoids of the High Himalayas (Frank, Thoni & Purtscheller, 1977; Mehta, 1977; Bhanot *et al.* 1979).

Biotite has been separated from one sample (K1) and the whole-rock biotite pair gives an age of 20.0±0.3 Ma (Table 5). This age is close to the muscovite and biotite ages from the Gumburanjon leucogranite (Ferrara *et al.* 1987; Villa & Oddone, 1988) and is interpreted as cooling age reflecting a regional phase of major uplift during Miocene time.

5.b. Zircon and monazite U–Th–Pb isotope results

Single crystal U–Th–Pb dating was performed on zircons and monazite extracted from small chips of orthogneiss 4326 and migmatized orthogneiss 4329 of the HHC. The results are listed in Table 6; sample descriptions and analytical details are given in Appendices B and C. In concordia representation (Fig. 6) the zircon data of the two rocks show contrasting patterns. The six zircon crystals from orthogneiss 4326 form a well-defined linear array (MSWD = 0.88) with concordia intercepts at 472+9/ −6 Ma and 0±90 Ma (York, 1969). The uncertainties of the ages are derived from the intercepts of the error envelopes (Ludwig, 1980) and are based on internal (propagated) errors at the 95% confidence level. The data points are moderately discordant; their relative positions along the discordia line are partly influenced by a correlation of grain size and Pb/U ratio, the largest zircon analysed (1 in Fig. 6 and Table 6) showing the highest ratio and the smallest grain analysed (4) the lowest ratio.

The data points of the five zircon crystals from migmatized orthogneiss 4329 (inset in Fig. 6) scatter to the right of a ≈ 500–630 Ma segment of the concordia curve. In contrast to the zircons from orthogneiss 4326, grain size and U concentration do not correlate. The scatter of the data points does not permit extrapolation of meaningful geological ages, though the apparent $^{207}Pb/^{206}Pb$ ages of ≈ 630–860 Ma suggest a Proterozoic minimum age for the oldest components present in the crystals.

The monazite grain from sample 4329 is characterized by rather high U and Th concentrations of 2.0

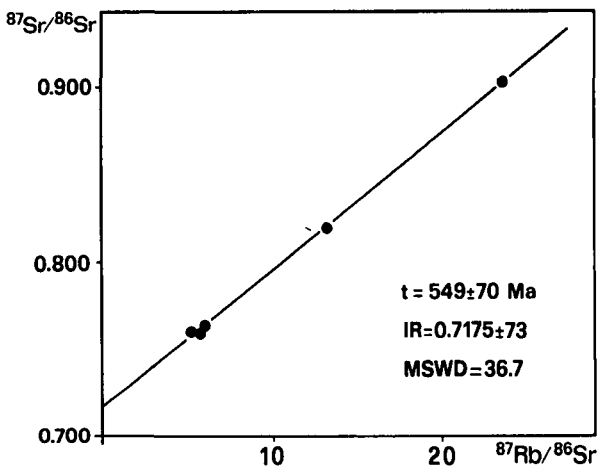

Figure 5. Rb–Sr whole-rock isochron of the Kade Unit metagranitoids reported in Tables 4 and 5. The isochron has been drawn without considering metagabbro K4.

Table 6. U–Th–Pb zircon and monazite isotope data for HHC orthogneisses 4326 and 4329

Sample	Type[a]	Size (μm)	Weight[b] (μg)	Th (ppm)	U (ppm)	Pb_{rad} (ppm)	Pb_{com} (ppm)	$^{206}Pb/^{204}Pb$[c] (observed)	Isotopic ratios corrected for blank and common Pb[e,f,g] $^{208}Pb/^{206}Pb$	$^{207}Pb/^{206}Pb$	$^{207}Pb/^{235}U$	$^{206}Pb/^{238}U$	P[d]	$^{208}Pb/^{232}Th$
Orthogneiss 4326: zircon data														
1	S11	440 × 140	21.7		847.5	58.50	1.1	2000	0.07121 ± 18	0.05645 ± 8	0.5541 ± 14	0.07119 ± 13	0.84	
2	S6–S7	350 × 90	9.2		1934	122.6	~ 0	5160	0.02820 ± 15	0.05646 ± 7	0.5293 ± 13	0.06799 ± 13	0.85	
3	S6–S7	290 × 80	7.4		2490	158.2	0.7	3190	0.01569 ± 17	0.05650 ± 9	0.5370 ± 18	0.06894 ± 19	0.88	
4	S2–S7	220 × 90	5.0		856.8	50.92	2.2	564	0.0359 ± 15	0.05641 ± 60	0.4923 ± 61	0.06329 ± 33	0.53	
5	S2	310 × 80	8.4		1296	85.18	0.5	1960	0.04569 ± 36	0.05653 ± 16	0.5409 ± 25	0.06939 ± 24	0.80	
6	S2–S7	300 × 100	8.1		2066	135.3	~ 0	3970	0.03601 ± 18	0.05655 ± 9	0.5437 ± 20	0.06974 ± 23	0.91	
Migmatized orthogneiss 4329: zircon and monazite data														
1	?	310 × 120	11.5		600.1	51.01	~ 0	2730	0.05514 ± 34	0.06758 ± 15	0.8206 ± 39	0.08806 ± 36	0.88	
2	S7	170 × 70	2.9		527.6	50.70	4	324	0.0634 ± 15	0.06588 ± 64	0.8989 ± 94	0.09896 ± 26	0.41	
3	S7	140 × 70	1.4		1031	77.79	1	342	0.0506 ± 27	0.0655 ± 11	0.711 ± 13	0.07864 ± 31	0.45	
4	S7–S8	140 × 50	1.5		1590	162.8	8	476	0.1663 ± 10	0.06335 ± 44	0.8455 ± 70	0.09680 ± 39	0.56	
5	S7–S9	200 × 70	2.4		1582	133.2	4	703	0.07846 ± 82	0.06064 ± 35	0.7186 ± 50	0.08594 ± 30	0.57	
Monazite			28.1	68230	20430	2073	2.3	23600	1.0329 ± 10	0.05603 ± 3	0.4348 ± 17	0.05627 ± 22	0.99	0.01684 ± 12

(a) Morphology after Pupin (1980). (b) Weighing errors are ±0.3 μg (95% confidence level). (c) Measured ratio corrected for mass fractionation and tracer contributions. (d) $^{207}Pb/^{235}U$ vs. $^{206}Pb/^{238}U$ correlation coefficient. (e) Quoted uncertainties (95% confidence level) refer to last significant digits of corresponding ratio. (f) The following Pb blank parameters were used for zircon (monazite) data reduction (uncertainties at 95% confidence level): total Pb = 17.0 ± 5.3 (20.6 ± 3.6) pg, $^{208}Pb/^{206}Pb$ = 2.057 ± 0.023 (2.080 ± 0.010), $^{207}Pb/^{206}Pb$ = 0.848 ± 0.015 (0.860 ± 0.006), $^{204}Pb/^{206}Pb$ = 0.0548 ± 0.0008 (0.0552 ± 0.0010); correlation coefficients for $^{208}Pb/^{206}Pb$ and $^{207}Pb/^{206}Pb$ vs. $^{204}Pb/^{206}Pb$ were 0.44 (0.13) and 0.60 (0.13), and 0.54 (−0.12), 0.51 (0.04) and 0.37 (−0.21) for ^{206}Pb content vs. $^{208}Pb/^{206}Pb$, $^{207}Pb/^{206}Pb$ and $^{204}Pb/^{206}Pb$, respectively. (g) Pb ratios used to correct for sample common Pb: $^{206}Pb/^{204}Pb$ = 18.00, $^{207}Pb/^{204}Pb$ = 15.62 and $^{208}Pb/^{204}Pb$ = 37.91 (Cumming & Richards, 1975, model III compositions for t = 480 Ma).

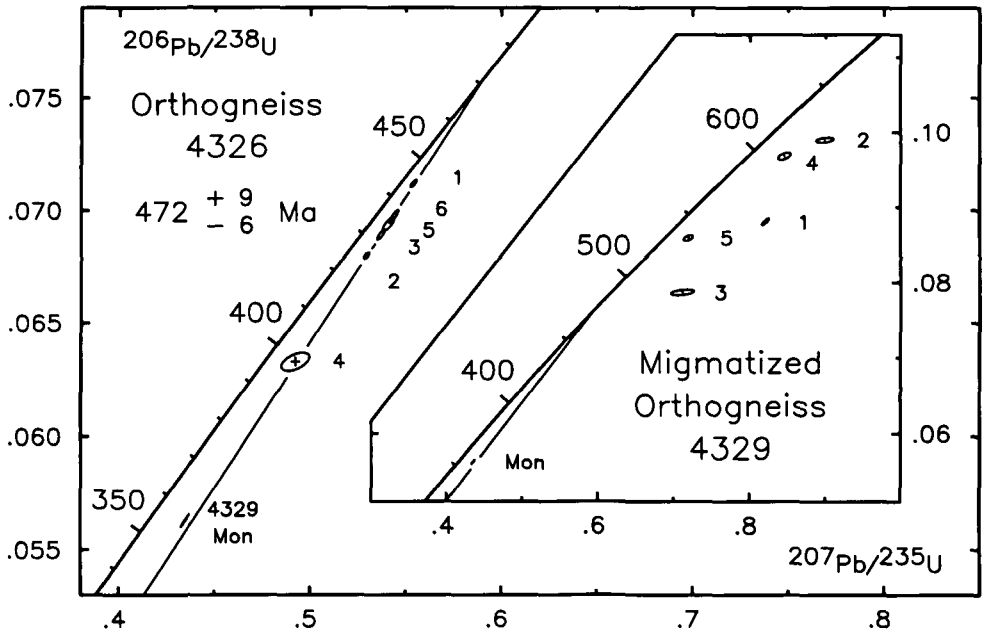

Figure 6. Concordia representation of zircon and monazite single crystal U–Pb data for HHC orthogneiss 4326 and migmatized orthogneiss 4329 (inset). The six zircon data points from sample 4326 define a discordia line (for reference also shown in the inset) intersecting the concordia curve at $472+9/-6$ Ma (age of emplacement) and 0 ± 90 Ma (overprint by Himalayan metamorphism). Further interpretations are given in the text.

and 6.8%, respectively. Its discordant Pb–U data point plots close to the best-fit line defined by the zircons from orthogneiss 4326, showing a considerably higher degree of discordance than the latter. A best-fit line connecting the data points of the six zircons from sample 4326 and the monazite data point intersects the concordia curve at 479 ± 4 Ma and 79 ± 13 Ma (95% confidence level by external errors; MSWD = 1.39). The intercept ages overlap within error limits with the ≈ 472 Ma age established by the zircon results alone, suggesting early Ordovician crystallization ages for both the zircon population of orthogneiss 4326 and the monazite crystal from sample 4329. The marked discordance of the monazite data point is interpreted to reflect high-grade metamorphic conditions associated with the Himalayan orogenic cycle. The similarity between Th/U = 3.21 (by weight) calculated from $(^{208}Pb/^{206}Pb)_{rad}$ and measured Th/U = 3.34 precludes major fractionation of Th/U during the Himalayan period and suggests that Pb loss rather than U and Th gain (by metamorphic overgrowth) was primarily responsible for the discordance.

In summary, our zircon and monazite U–Th–Pb results establish a Lower Palaeozoic age for the HHC orthogneisses. The influence of Himalayan high-grade metamorphism, which according to field relations appears to be responsible for the migmatization of orthogneiss 4329, is recorded by the discordance of its monazite data point and the discordance of the zircon data from the orthogneiss 4326. The contrasting U–Pb data patterns of the zircon populations from the two samples result from the presence of inherited Precambrian components in the zircons of 4329 and their virtual absence in sample 4326 at the time of protolith emplacement during Lower Palaezoic time; overprint by a high-grade Himalayan event finally led to the presently observed data patterns.

6. Discussion and conclusions

6.a. Age of the magmatic and metamorphic events in the High Himalayas

The interpretation that the very low-grade sedimentary sequences of Precambrian–early Tertiary age of the Tibetan zone represent the stratigraphic cover of the High Himalayan crystalline rocks, led some authors to ascribe most of the magmatic and metamorphic events recorded by the crystalline rocks to a pre-Himalayan (Precambrian) history (e.g. Srikantia *et al.* 1980; Thakur, 1980; Fuchs, 1988). Conversely, evidence that nappe tectonics is widespread and major thrusts or faults occur in Zanskar between the crystalline rocks and the Tibetan sequences (e.g. Baud *et al.* 1984; Gaetani, Garzanti & Jadoul, 1985; Searle, 1986; Herren, 1987; Baud, 1988), led other authors to attribute the metamorphic evolution and the intrusive rocks of the High Himalayan Crystallines (HHC) to the Tertiary post-collisional history (e.g. Searle & Fryer, 1986). The present work proves conclusively the existence of a pre-Himalayan magmatic cycle and of Tertiary leucogranites (Fig. 7).

The *pre-Himalayan intrusives* occur both in the HHC and in the Kade Unit. U–Th–Pb dating of

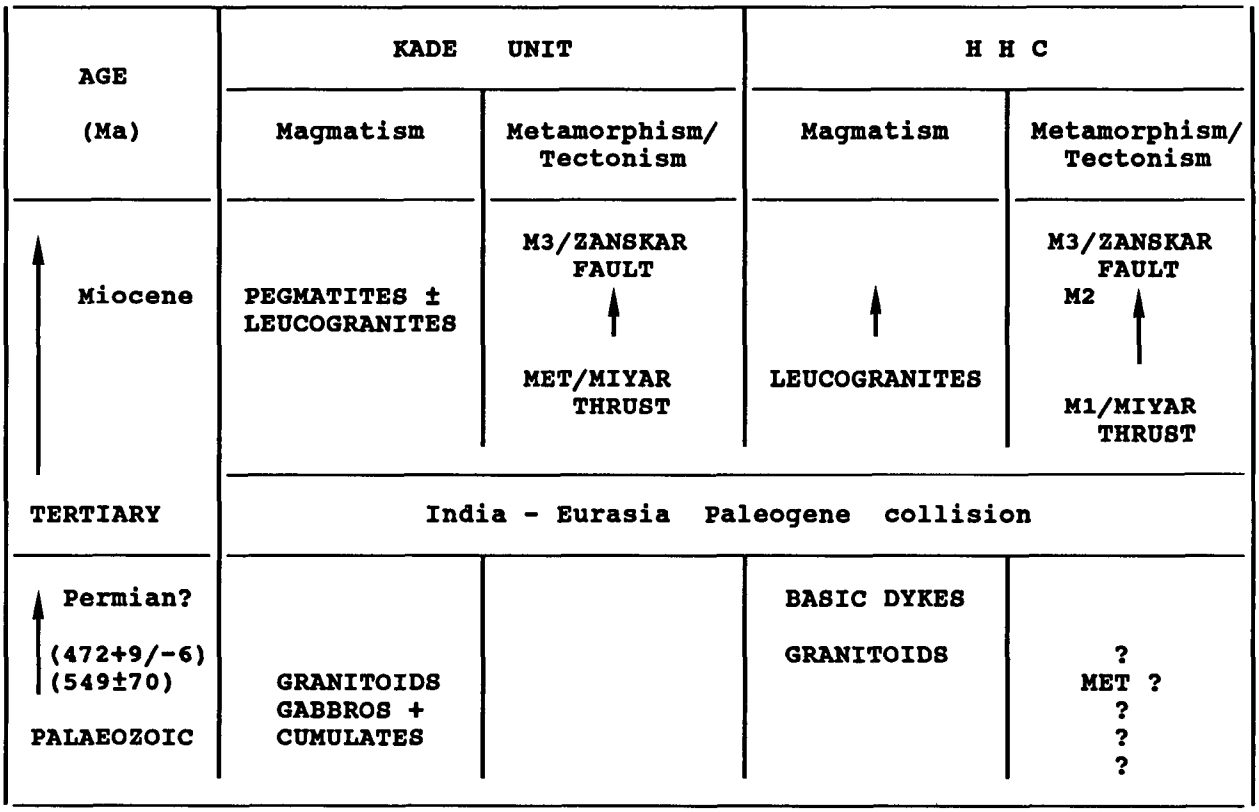

Figure 7. Magmatism, metamorphism and tectonism in the Lahul–Zanskar region (see text for discussion).

zircons and monazite establishes an early Palaeozoic age (472+9/−6 Ma) for the granitoids of the HHC which were later converted to orthogneisses and migmatites (section 5.b). In the Kade Unit, granitoids later transformed to low-grade orthogneisses give a Rb–Sr whole-rock age of 549±70 Ma and $^{87}Sr/^{86}Sr$ initial composition of ≈ 0.718 (section 5.a). For the Kade Unit, the ophitic and porphyritic structures preserved in gabbros and the existence of cumulus olivine and spinel in cumulates associated with the granitoids are consistent with shallow-level intrusions into a sedimentary sequence.

Comparable early-Palaeozoic ages have been obtained for other granitoids of the High Himalayas by Frank, Thoni & Purtscheller (1977), Mehta (1977), Bhanot *et al.* (1979), Le Fort, Debon & Sonet (1980) and Ferrara, Lombardo & Tonarini (1983). This is in agreement with observations by Honegger *et al.* (1982), Pognante *et al.* (1987), Kündig (1989) and Pognante & Lombardo (1989), who emphasized the abundance of pre-Himalayan orthogneisses forming large bodies and transposed dykes within the HHC paragneisses of the Zanskar region.

Furthermore a pre-Himalayan magmatism in the Lahul–Zanskar region is also recorded by the dykes and small bodies of porphyritic basic rocks which injected the HHC granitoids prior to Himalayan metamorphism. Though geochronological and geochemical data on these rocks are still lacking, they might hypothetically belong to the Permian magmatism which formed the Panjal Trap, as suggested by Greco (1988) for some dykes of the HHC in Pakistan (Fig. 7).

Though subordinate relative to the pre-Himalayan granitoids, the *Tertiary leucogranites and pegmatites* are much more abundant in the HHC than in the Kade Unit. For the Gumburanjon leucogranite body, Sr isotope disequilibrium prevents applying the whole-rock isochron method (Ferrara *et al.* 1987), while $^{39}Ar/^{40}Ar$ data on micas give ages around 19 Ma (Villa & Oddone, 1988). In the high-grade zones, leucogranite formation appears to be linked to migmatization of the early Palaeozoic granitoids which often include quartzofeldspathic leucosomes mixed with leucogranite layers. These layers probably represent a first generation of leucogranites which may have formed during active tectonism and pervasive deformation under partly molten conditions. They are intruded by dykes and lens-shaped bodies of leucogranites which also crosscut the main regional foliation. Like the other leucogranites of the Himalayan belt (Le Fort, 1986; Searle & Fryer, 1986; Castelli & Lombardo, 1988), the arguments reported above and the high $^{87}Sr/^{86}Sr$ ratios of the Gumburanjon body (0.747–0.775; Ferrara *et al.* 1987), are consistent with generation by anatexis in the high-grade zone of the HHC and with a Miocene age of emplacement for the Lahul–Zanskar leucogranites.

As regards the *polyphase metamorphic recrystallization* of the HHC characterized by two main stages (M1 and M2), a Tertiary Himalayan age and a major phase of uplift during Miocene time are inferred by: (1) the geochronological data which give Rb–Sr ages ranging from 29 to 21 Ma for muscovites and from 21 to 11 Ma for biotites (Frank, Thoni & Purtscheller, 1977; Mehta, 1977; Honegger *et al.* 1982; section 5.a); (2) the close relations between metamorphism and deformation in some Himalayan thrust zones (e.g. Miyar Thrust); (3) the involvement in the metamorphism of stratigraphically dated sequences of Mesozoic age like the Jurassic metasediments of Tandi (Powell & Conaghan, 1973).

However, a few inconsistencies with a purely Himalayan age of some M1 metamorphic assemblages recorded by the HHC arise from detailed study of some metabasics, which are intruded by the early Palaeozoic granitoids and show relics of high-pressure granulite assemblages (Fig. 4; Table 3; Pognante & Lombardo, 1989). If these relics do not record disequilibrium relations or an early stage of the Himalayan metamorphism which is now overprinted in the other rock types of the HHC, they should be ascribed to an older metamorphic event incompletely obliterated by Himalayan recrystallizations (Fig. 7).

More evidence of a pre-Himalayan metamorphism in the collided Indian plate has been recently provided by Baig *et al.* (1988) and Williams, Treloar & Coward (1988). Furthermore, the presence of a magmatic and, perhaps, metamorphic event of early Palaeozoic age in the HHC is consistent with data concerning the sediments of the Tibetan nappes; the sedimentary data provide evidence of a Cambro-Ordovician orogenic event in northwestern Himalaya (Garzanti, Casnedi & Jadoul, 1986).

6.b. Metamorphism, tectonism and leucogranite emplacement during the formation of the High Himalayan belt

The main results of the present study concerning the Himalayan metamorphic–tectonic history are summarized as follows (Fig. 7):

(1) A syn-metamorphic tectonic discontinuity defined as the Miyar Thrust occurs within the High Himalayas of the Lahul–Zanskar region and separates the structurally lower HHC from the upper Kade Unit.

(2) A metamorphic gap exists along the Miyar Thrust between the medium/high-grade HHC and the low-grade Kade Unit.

(3) A metamorphic zonation with a decrease in grade of the metamorphic assemblages toward the Miyar Thrust exists in the HHC and, less evident, in the Kade Unit. More or less comparable zonations have been reported at the top of the HHC near the Zanskar Fault (Honegger *et al.* 1982; Herren, 1987; Pognante & Lombardo, 1989; Searle & Rex, 1989) and at the base of the HHC near the Main Central Thrust and the Lesser Himalaya (Stäubli, 1989).

(4) The high-grade zones occur at middle structural levels in the HHC and are characterized by advanced migmatization, centimetre-size sillimanite aggregates in gneisses and scattered orthopyroxene-biotite-bearing metamorphic assemblages in metabasics. In the high-grade HHC gneisses, a climax-stage M1 (T = 650–750 °C; $P \approx$ 6–8 kbar) was followed by a retrograde recrystallization M2 at decreasing pressures.

(5) Along the Miyar Thrust and in the rocks of the upper HHC levels, stage M1 is coeval with mylonitization, is characterized by medium-grade assemblages ($T \approx$ 500–600 °C, $P \approx$ 6–8 kbar) and was followed by a pressure drop at more or less increasing temperatures (M2); no evidence of pre-mylonitic high-grade assemblages have been found in these medium-grade rocks.

(6) A later very low-grade recrystallization M3 is localized along the Zanskar Fault; it records a shallow level tectonism which reactivates – or truncates at low angle – an older ductile shear zone similar to the Miyar Thrust and post-dates leucogranite intrusion.

The data discussed above and the P–T paths reported in Figure 4 are indicative of a *polyphase tectonic–metamorphic history during exhumation* from relatively deep crustal levels linked to the post-collisional evolution of the Indian plate. As regards *metamorphic zonations* and inverted metamorphic gradients in the High Himalayas, they have been ascribed either to thermal interaction between 'hot' and 'cold' tectonic units (Le Fort, 1975), or to syn/post-metamorphic large-scale deformation of the isograds (Frank, Thoni & Purtscheller, 1977; Searle & Rex, 1989).

The close relations between Miyar Thrust and metamorphic zonation, and the lack of obvious large recumbent folds in the studied Lahul–Zanskar region, favour Le Fort's model (1975); however, the metamorphic gap between HHC and Kade Unit implies further post-M1 displacements along the Miyar Thrust. This has been already suggested by Caby, Pecher & Le Fort (1983), Brunel & Kienast (1986), Hodges & Silverberg (1988) and Stäubli (1989) for the Main Central Thrust at the base of the HHC. Such a post-M1 phase of thrusting is in agreement with deformation of Miocene leucogranites which, close to the Miyar Thrust, crosscut M1 foliation.

Consequently, we propose that during intracontinental thrustings in the Indian plate, the HHC was stacked with cooler nappes represented by the Lesser Himalaya below the Main Central Thrust (Stäubli, 1989), and the Kade Unit above the Miyar Thrust. Stacking and exhumation occurred not only along the above cited thrusts, but very likely also along the mylonites describes by Kündig (1989) within the HHC. In the migmatized zones of the HHC, rapid

movements of crustal blocks may have been enhanced by formation of melt-lubricated shear zones according to the mechanism proposed by Hollister & Crawford (1986). In response to thermal conductivity, recrystallization M1 took place at relatively low temperatures in the HHC close to the tectonic boundaries with the adjacent cooler nappes; in contrast, in the middle structural levels characterized by the abundance of orthogneisses rich in zircon, monazite and apatite, temperatures increased possibly in response to high radioactive heat production as discussed by Pinet & Jaupart (1987). Because of the lack of pre-M1 high-grade relics, temperatures at the top of the HHC should never have reached the high values of the middle structural levels; alternatively, the higher temperature assemblages were completely obliterated during subsequent recrystallizations.

The crustal-derived leucogranites of Miocene age also played an important role in the tectonic-metamorphic history of the studied region. As discussed above, these rocks generated by anatexis in the high-grade zone of the HHC, while partial melting may have been induced by high radioactive heat production (Pinet & Jaupart, 1987) with the probable contribution of rising fluids from the underlying low-grade metasediments of the Lesser Himalaya (Le Fort, 1981). Intrusion of a first generation of concordant leucogranites, perhaps starting from stage M1, may have weakened the HHC rocks and hence favoured crustal displacements (Hollister & Crawford, 1986). At upper structural levels leucogranite intrusion probably occurred during or just before stage M2 and may have contributed to the temperature rise following stage M1 (Fig. 4). On the other hand, the progressive temperature decrease upward in the HHC during stage M1, may be the reason for the scarcity or the lack of leucogranites in the Kade Unit. In conclusion, leucogranite intrusion in the upper levels was more or less coeval with stage M2 and the latest movements along the Miyar Thrust, but pre-dated juxtaposition of the Tibetan nappes along the Zanskar Fault.

Acknowledgements. Discussions and reviews by M. Gaetani, E. Garzanti, B. Lombardo and M. Searle are much appreciated. P.B., D.C., G.G. and U.P. acknowledge the Ministero della Pubblica Istruzione (grant 40% to M. Gaetani and U. Pognante, 1985, 1986) and the C.S. sui Problemi dell'Orogeno delle Alpi Occidentali (C.N.R., Torino) for financial support. The C.S. Stratigrafia e Petrografia delle Alpi Centrali (C.N.R., Milano) is acknowledged for installation and operation of the electron microprobe laboratory in the Dipartimento di Scienze della Terra of Milano. F.O. and M.M. thank I. Ivanov and S. Barth for help with mineral preparation.

Appendix A. List of abbreviations

ab = albite, AS = Al-silicate, alm = almandine, am = green amphibole, an = anorthite, and = andalusite, bi = biotite, cc = calcite, ch = chlorite, cpx = clinopyroxene, ct = chloritoid, ecl = eclogite, ep = epidote, gra = granulite, gt = garnet, hbl = hornblende, Kf = K-feldspar, ky = kyanite, ms = muscovite, opx = orthopyroxene, pl = plagioclase, qtz = quartz, sill = sillimanite, sph = sphene, st = staurolite, to = tourmaline, zr = zircon; HHC = High Himalayan Crystallines, IR = initial ratio, L = liquid, P = pressure, T = temperature, t = time, WR = whole-rock.

Appendix B. Location and mineralogy of the investigated samples

V1637: metabasite (Miyar valley, front of Miyar glacier, 4100 m): opx, am, pl, bi, cpx. V1678: paragneiss close to the Miyar Thrust (Miyar valley, Gumba Nala, 4500 m): qtz, bi, ms, ab, gt, to. V1726: mylonitic gneiss close to the Miyar Thrust (Miyar valley, front of Miyar glacier, 4600 m): qtz, ms, bi, gt, st, ms, pl. V1731: migmatized gneiss (Kang-La, 5300 m): qtz, bi, pl, sill, Kf. K1: orthogneiss (Kade valley, Jankar Sumdo, 3900 m): qtz, ab, Kf, bi, ep, ms, zr. K2: orthogneiss (same location as K1): qtz, ab, Kf, bi, ms, ep, sph, zr. K3: orthogneiss (same location as K1): qtz, ab, Kf, bi, ms, ep, zr. K4: metagabbro (same location as K1): am, ab, ep, bi, sph, ch. K6: orthogneiss (Kade valley, northwest Darcha, 3600 m): qtz, Kf, ab, ms, bi, ch, cc. K7: orthogneiss (same location as K6, 3500 m): qtz, kf, ab, bi, ms, ep, sph. 4326: orthogneiss (Temasa valley, 3950 m): qtz, pl, Kf, bi, ms, ch, zr. 4329: migmatized orthogneiss (Temasa valley, 4000 m): qtz, pl, Kf, ms, bi, gt, zr.

Appendix C. Analytical details concerning U-Th-Pb isotope investigation

Analytical procedures. Logistic problems associated with remote-area field work restricted rock samples available for zircon and monazite dating to 71 g for orthogneiss 4326 and 41 g for migmatized orthogneiss 4329, respectively, calling for application of low-level techniques for Th–U–Pb isotope analysis. Zircon and monazite were extracted by standard procedures. For detailed microscopic examination by transmitted light and final selection, the zircons were mounted in glycerine. To reduce common Pb content and to assess chemical stability of zircon and monazite crystals, acid-leaching procedures similar to those described in Bossart *et al.* (1986) were applied prior to sample decomposition. The HCl leach solutions of zircons 1 and 6 from sample 4326 and 3 from sample 4329 were analysed for U and Pb content and Pb isotopic composition. The leaching procedure removed merely $\approx$ 0.01–0.04% of their original U and $\approx$ 0–0.03% of their radiogenic Pb contents. Amounts of common Pb leached were non-trivial, reaching $\approx$ 10–100% per sample common Pb (i.e. common Pb remaining after correction for analytical blank). For monazite, Th, U, radiogenic Pb and common Pb measured in the combined HNO_3 and HCl leach solution amounted to 0.17, 0.14, 0.14 and 30% of the respective original contents in the monazite. All samples were spiked prior to decomposition with a mixed ^{233}U–^{235}U–^{230}Th–^{205}Pb tracer. Procedures for zircon decomposition, U and Pb extraction and mass spectrometry followed closely those given in Bossart *et al.* (1986). Monazite was decomposed in 0.3 ml 6 M HCl (7 day at 215 °C) using PTFE bomb techniques (Krogh, 1973). Th, U and Pb extraction and mass spectrometry were performed as described in Barth, Oberli & Meier (1989).

Mineralogical characteristics. The zircon populations of both orthogneiss samples consist predominantly of elongate

and colourless crystals enclosing varying amounts and types of inclusions. Typical indicators for inherited cores, however, were not observed. The edges of most grains are slightly rounded. The morphologies of the crystals analysed for U–Pb were determined by the method of Pupin (1980) and are listed in Table 6. The zircons analysed from orthogneiss 4326 and migmatized orthogneiss 4329 cover fields S2–S6–S7–S11 and S7–S8–S9 in Pupin's diagram, respectively, which are close to or overlap with those typically associated with zircons from anatectic granites and migmatites (Pupin, 1980). The monazite grain analysed from sample 4329 was characterized by greenish colour and essentially anhedral morphology suggestive of resorption.

References

Baig, M. S., Lawrence, R. D. & Snee, L. W. 1988. Evidence for late Precambrian to early Cambrian orogeny in northwest Himalaya, Pakistan. *Geological Magazine* **125**, 83–6.

Barth, S., Oberli, F. & Meier, M. 1989. Age and U–Th–Pb systematics of zircon and allanite; a high resolution isotopic study of the Periadriatic Rensen Pluton (Northern Italy). *Earth and Planetary Science Letters* (submitted).

Baud, A. 1988. The nappe and thrust tectonics in Zanskar area (NW Himalaya), review of the so called 'autochthony' of the Tethys-Tibetan zone. *Himalayan–Karakoram–Tibet Workshop Meeting, Lausanne*, 43–4.

Baud, A., Gaetani, M., Garzanti, E., Nicora, A. & Tintori, A. 1984. Geological observations in south-eastern Zanskar and adjacent Lahul area (northwestern Himalaya). *Eclogae Geologicae Helvetiae* **77**, 171–97.

Bhanot, V. B., Bhandari, A., Singh, V. P. & Kansal, A. K. 1979. Geochronological and geological studies on a granite of High Himalaya, Northeast of Manikaran, Himachal-Pradesch. *Journal of the Geological Society of India* **20**, 90–4.

Bossart, P. J., Mejer, M., Oberli, F. & Steiger, R. H. 1986. Morphology versus U–Pb systematics in zircon: a high resolution isotopic study of a zircon population from a Variscan dike in the Central Alps. *Earth and Planetary Science Letters* **78**, 339–54.

Brunel, M. & Kienast, J. R., 1986. Etude petro-structurale des chevauchements ductiles himalayens sur la trasversale de l'Everest-Makalu (Nepal oriental). *Canadian Journal of Earth Sciences* **23**, 1117–37.

Caby, R., Pecher, A. & Le Fort P., 1983. Le grand chevauchement central himalayen: nouvelles données sur le metamorphisme inverse à la base de la Dalle du Tibet. *Revue de Géologie dynamique et de Géographie Physique* **24**, 89–100.

Castelli, D. & Lombardo, B. 1988. The Gophu La and Western Lunana granites: Miocene muscovite leucogranites of the Bhutan Himalaya. *Lithos* **21**, 211–25.

Cumming, G. L. & Richards, J. R. 1975. Ore lead isotope ratios in a continuously changing earth. *Earth and Planetary Science Letters* **28**, 155–71.

Ellis, D. J. & Green, D. H. 1979. An experimental study of the effect of Ca upon garnet–clinopyroxene Fe–Mg exchange equilibria. *Contributions to Mineralogy and Petrology* **71**, 13–22.

Ferrara, G., Lombardo, B. & Tonarini, S. 1983. Rb/Sr geochronology of granites and gneisses from the Mount Everest Region, Nepal Himalaya. *Geologische Rundschau* **72**, 119–36.

Ferrara, G., Lombardo, B., Tonarini, S. & Turi, B. 1987. New Rb/Sr data on granitoids from Gumburanjon and Kade Chu (High Himalaya). *Himalayan–Karakoram Workshop Meeting, Nancy*, 33.

Ferry, J. M. & Spear, F. S. 1978. Experimental calibration of the partitioning of Fe and Mg between biotite and garnet. *Contributions to Mineralogy and Petrology* **66**, 113–17.

Frank, W., Hoinkes, G., Miller, C., Purtscheller, F., Richter, W. & Thoni, M. 1973. Relations between metamorphism and orogeny in a typical section of Indian Himalayas. *Tschermaks Mineralogische und Petrographische Mitteilugen* **20**, 303–32.

Frank, W., Thoni, M. & Purtscheller, F. 1977. Geology and petrology of Kulu–South Lahul area. *Colloquie International C.N.R.S. no.* 268: *Ecologie et Géologie de l'Himalaya, Sèvres*, 1976, 147–72.

Fuchs, G. 1988. Arguments for the autochthony of the Tibetan Zone. *Himalayan-Karakoram-Tibet Workshop Meeting, Lausanne*, 41.

Gaetani, M., Garzanti, E. & Jadoul, F. 1985. Main structural elements of Zanskar, Nw Himalaya (India). *Rendiconti della Società Geologica Italiana* **8**, 3–8.

Garzanti, E., Casnedi, R. & Jadoul, F. 1986. Sedimentary evidence of a Cambro-Ordovician orogenic event in the northwestern Himalaya. *Sedimentary Geology* **48**, 237–65.

Greco. A. 1988. Tectonics and metamorphism in the Himalayas of NE Pakistan (Kaghan valley and Azad Kashmir). *Himalayan-Karakoram-Tibet Workshop Meeting, Lausanne*, 24–5.

Green, T. & Ringwood, A. E. 1967. An experimental investigation of the gabbro-eclogite transformation and some petrological applications. *Geochimica and Cosmochimica Acta* **31**, 767–833.

Herren, E. 1987. The Zanskar shear zone: northeast-southwest extension within the Higher Himalayas (Ladakh, India). *Geology* **15**, 409–13.

Hodges, K. & Silverberg, D. S. 1988. Thermal evolution of the greater Himalaya, Garhwal, India. *Tectonics* **7**, 583–600.

Hollister, L. S. & Crawford, M. L. 1986. Melt-enhanced deformation: a major tectonic process. *Geology* **14**, 555–61.

Honegger, K., Dietrich, V., Frank, W., Gansser, A., Thoni, M. & Trommsdorff, V. 1982. Magmatism and metamorphism in the Ladakh Himalayas (the Indus–Tsangpo suture zone). *Earth and Planetary Science Letters* **60**, 253–92.

Hoschek, G. 1969. The stability of staurolite and chloritoid and their significance in the metamorphism of pelitic rocks. *Contributions to Mineralogy and Petrology* **22**, 208–32.

Krogh, T. E. 1973. A low-contamination method for hydrothermal decomposition of zircon and extraction of U and Pb for isotopic age determinations. *Geochimica et Cosmochimica Acta* **37**, 485–94.

Kündig, R. 1989. Domal structures and high grade metamorphism in the Higher Himalayan Crystalline–Zanskar region (NW India). *Journal of Metamorphic Geology* **7**, 43–55.

Leake, B. E. 1978. Nomenclature of amphiboles. *American Mineralogist* **63**, 1023–52.

Le Fort, P. 1975. Himalaya: the collided range – Present

knowledge of the continental arc. *American Journal of Science* **275A**, 1–44.

LE FORT, P. 1981. Manaslu leucogranite: a collision signature of the Himalaya – A model for its genesis and emplacement. *Journal of Geophysical Research* **86**, 10545–68.

LE FORT, P. 1986. Metamorphism and magmatism during the Himalayan collision. In *Collision Tectonics* (ed. M. P. Coward and A. C. Ries), pp. 159–72. Geological Society Special Publication no. 19.

LE FORT, P., DEBON, F. & SONET, J. 1980. The 'Lesser Himalayan' cordierite granite belt, typology and age of the pluton of Mansehra, Pakistan. *Special Issue of the Geological Bulletin of the University of Peshawar* **13**, 51–61.

LUDWIG, K. R. 1980. Calculation of uncertainties of U–Pb isotope data. *Earth and Planetary Science Letters* **46**, 212–20.

LUDWIG, K. R. 1988. *A plotting and regression program for radiogenic-isotope data for IBM-PC compatible computers*. USGS Open-File report no. 88–557.

MEHTA, P. K. 1977. Rb/Sr geochronology of the Kulu–Mandi belt: its implications for the Himalayan Tectogenesis. *Geologische Rundschau* **66**, 156–75.

MERRILL, R. B., ROBERTSON, J. K. & WYLLIE, P. J. 1970. Melting reactions in the system $NaAlSi_3O_8$–$KAlSi_3O_8$–SiO_2–H_2O to 20 kilobars compared with results for other feldspar–quartz–H_2O and rock–H_2O systems. *Journal of Geology* **78**, 558–69.

MUELLER, R. F. & SAXENA, S. K. 1977. *Chemical Petrology*. New York Heidelberg Berlin: Springer-Verlag. 394pp.

NEWTON, R. C. & HASELTON, H. T. 1981. Thermodynamics of the garnet–plagioclase–Al_2SiO_5–quartz geobarometer. In *Thermodynamics of Minerals and Melts* (ed. R. C. Newton, A. Navrotsky and B. J. Wood), pp. 129–45. New York: Springer-Verlag.

NEWTON, R. C. & PERKINS, D. 1982. Thermodynamic calibration of geobarometers based on the assemblages garnet–plagioclase–orthopyroxene (clinopyroxene)–quartz. *American Mineralogist* **67**, 203–22.

PINET, C. & JAUPART, C. 1987. A thermal model for the distribution in space and time of the Himalayan granites. *Earth and Planetary Science Letters* **84**, 87–99.

POGNANTE, U. & LOMBARDO, B. 1989. Metamorphic evolution of the High Himalayan Crystallines in SE Zanskar, India. *Journal of Metamorphic Geology* **7**, 9–17.

POGNANTE, U., GENOVESE, G., LOMBARDO, B. & ROSSETTI, P. 1987. Preliminary data on the High Himalayan Crystallines along the Padum–Darcha Traverse (South-Eastern Zanskar, India). *Rendiconti della Società Italiana di Mineralogia e Petrologia* **42**, 95–105.

POWELL, C. M. A. & CONAGHAN, P. J. 1973. Polyphase deformation in Phanerozoic rocks of the central Himalayan gneiss, northwest India. *Journal of Geology* **81**, 127–43.

PUPIN, J. P. 1980. Zircon and granite petrology. *Contributions to Mineralogy and Petrology* **73**, 207–20.

RAO, B. B. & JOHANNES, W. 1979. Further data on the stability of staurolite + quartz and related assemblages. *Neues Jahrbuch für Mineralogie Abhandlungen* **10**, 437–47.

RICHARDSON, S. W. 1968. Staurolite stability in a part of the system Fe–Al–Si–O–H. *Journal of Petrology* **9**, 468–88.

SEARLE, M. P. 1986. Structural evolution and sequence of thrusting in the High Himalayan, Tibetan-Tethys and Indus suture zones of Zanskar and Ladakh, Western Himalaya. *Journal of Structural Geology* **8**, 923–36.

SEARLE, M. P. & FRYER, B. J., 1986. Garnet, tourmaline and muscovite-bearing leucogranites, gneisses and migmatites of the Higher Himalayas from Zanskar, Kulu, Lahoul and Kashmir. In *Collision Tectonics* (eds M. P. Coward and A. C. Ries), pp. 185–201. Geological Society of London Special Publication no. 19.

SEARLE, M. P. & REX, A. J. 1989. Thermal model for the Zanskar Himalaya. *Journal of Metamorphic Geology* **7**, 127–34.

SRIKANTIA, S. V., GANESAN, T. M., RAO, R. N., SINHA, P. H. & TIRKEY, P., 1980. Geology of the Zanskar area, Ladakh Himalaya. *Himalayan Geology* **8**, 1009–33.

STÄUBLI, A. 1989. Polyphase metamorphism and the development of the Main Central Thrust (M.C.T.) at the Kishtwar window (NW India). *Journal of Metamorphic Geology* **7**, 73–93.

STEIGER, R. H. & JÄGER, E. 1977. Subcommission on Geochronology: convention on the use of decay constants in geo- and cosmochronology. *Earth and Planetary Science Letters* **36**, 359–62.

STORRE, B. & KAROTKE, E. 1971. An experimental determination of the upper stability limit of muscovite + quartz in the range 7–20 kb water pressure. *Neues Jahrbuch für Mineralogie Monatshefte* **115**, 237–40.

THAKUR, V. C. 1980. Tectonics of the central crystallines of western Himalaya. *Tectonophysics* **62**, 141–54.

THAKUR, V. C. 1987. Plate tectonic interpretation of the Western Himalaya. *Tectonophysics* **134**, 91–102.

TRACY, R. J. 1982. Compositional zoning and inclusions in metamorphic minerals. In *Characterization of Metamorphism through Mineral Equilibria* (ed. J. M. Ferry), pp. 355–97. Mineralogical Society of America: Reviews in Mineralogy Series no. 10.

TRELOAR, P. J., WILLIAMS, M. P., COWARD, M. P., BROUGHTON, R. D. & WINDLEY, B. F. 1989. Deformation, metamorphism and imbrication of the Indian plate, south of the Main Mantle Thrust, north Pakistan. *Journal of Metamorphic Geology* **7**, 111–25.

ULMER, P. 1986. *NORM-program for cation and oxygen mineral norms*. Computer Library IKP-ETH, Zürich.

VILLA, I. & ODDONE, M. 1988. $^{39}Ar/^{40}Ar$ ages of Himalayan leucogranites decrease eastward. *Himalayan–Karakoram–Tibet Workshop Meeting, Lausanne*, 1988, 16.

WILLIAMS, M. P., TRELOAR, P. J. & COWARD, M. P. 1988. More evidence of pre-Himalayan orogenesis in Northern Pakistan. *Geological Magazine* **125**, 651–2.

YORK, D. 1969. Least squares fitting of a straight line with correlated errors. *Earth and Planetary Science Letters* **5**, 320–4.